stellarator news

Published by Fusion Energy Division, Oak Ridge National Laboratory
Building 9201-2 P.O. Box 2009 Oak Ridge, TN 37831-8071, USA

Editor: James A. Rome Issue 88 September 2003
E-Mail: jar@ornl.gov Phone (865) 574-1306
On the Web at *http://www.ornl.gov/fed/stelnews*

Conceptual Design Review of QPS

The Quasi-Poloidal Stellarator (QPS) passed a crucial milestone in June 2003 with the completion of a successful Conceptual Design Review. The review was conducted by a panel of distinguished experts from the fusion community and the U.S. Department of Energy (DOE): David Anderson (Univ. Wisconsin), Robert Baldi (General Atomics), James Carney (DOE), Jeffrey Harris (Australian National Univ.), Stephen Knowlton (Auburn Univ.), Hutch Neilson (Princeton Plasma Physics Laboratory), Gregory Pitonak (DOE), Wayne Reiersen (Princeton Plasma Physics Laboratory), and Harold Weitzner (New York Univ.).

The panel examined all aspects of the QPS project — physics, engineering, cost, schedule, and management. The panel expressed the opinion that the project could meet the QPS technical mission and could manufacture and construct the critical systems. The panel recommended some actions for the next step in the DOE approval process (CD-1, which will permit project funds to be expended on QPS), and made some longer-term recommendations for each area. QPS is following an approval process parallel to that for the National Compact Stellarator Experiment (NCSX). A panel of plasma physicists and engineers had previously conducted a Physics Validation Review of the QPS design and concluded that the physics approach to the QPS design was appropriate for a concept exploration experiment.

QPS will complement NCSX to complete the experimental basis necessary to advance the compact stellarator concept to the next stage of development. The mission of QPS is to broaden understanding of toroidal magnetic configurations and develop understanding of the key issues for the low-aspect-ratio quasi-poloidal approach to a high-beta compact stellarator concept. The next step in the QPS project is R&D and more detailed design of the QPS components. The fabrication project is planned to start in October 2004 and finish in early 2008 at a cost of $20M. The facility will be sited at Oak Ridge National Laboratory.

Details of the QPS and the Conceptual Design Report can be found at http://qps.fed.ornl.gov/.

J. F. Lyon
Oak Ridge National Laboratory
Oak Ridge, TN 37831 USA
E-mail: lyonjf@ornl.gov

Stellarator News URL to move

Because the ORNL public Web servers will be replaced with new hardware, beginning October 20, the URL of *Stellarator News* will change to

http://www.ornl.gov/sci/fed/stelnews

In this issue . . .

Stellarator flexibility options with variable modular coil currents

Recently developed stellarator optimization tools [1] have successfully merged the external coil-plasma boundary optimization with the internal plasma boundary physics optimization steps. Besides allowing better control over the engineering features and complexity of the magnet coils (and thus lower cost) in an ongoing design, this procedure also allows one to explore more methodically the physics flexibility options in a completed design for which the coil geometry has become fixed, but the coil currents can still be varied over some specified range. This type of flexibility is one of the significant advantages that stellarators can offer over tokamaks. Developing better tools for exploring the available parameter space can enhance the scientific value of a stellarator experiment.

As an example of such flexibility studies, we analyze the Quasi-Poloidal Stellarator (QPS) device [2], which has been designed with independent power supplies for controlling the five unique modular coil groups, the three vertical field coil pairs, and the toroidal field coils. In addition, the plasma current can be considered as an independent variable, because an Ohmic transformer is available to drive plasma current. After using one of the modular coil currents as a normalizing parameter, there are still nine independent parameters. Since searches of even a nine-dimensional parameter space, based on intuition or trial and error, are likely to miss interesting combinations, we have used the merged coil-plasma optimizer code to automate this search process. In the following, we focus on transport improvement and island avoidance at low plasma pressure (beta), but such techniques can also be applied to stability optimization targets at finite beta.

Coil configuration

QPS is a compact ($R_0/\langle a\rangle = 2.7$), two-field period stellarator that maintains a dominant poloidal symmetry in its magnetic field strength variation. The current reference design for QPS is based on a set of 20 modular field coils (with 5 unique coil shapes), 6 vertical field coils, and 12 toroidal field coils. In Fig. 1, the full set of coils is shown along with the plasma outer flux surface. Figure 2 shows only the plasma outer flux surface for the reference configuration and the modular coils.

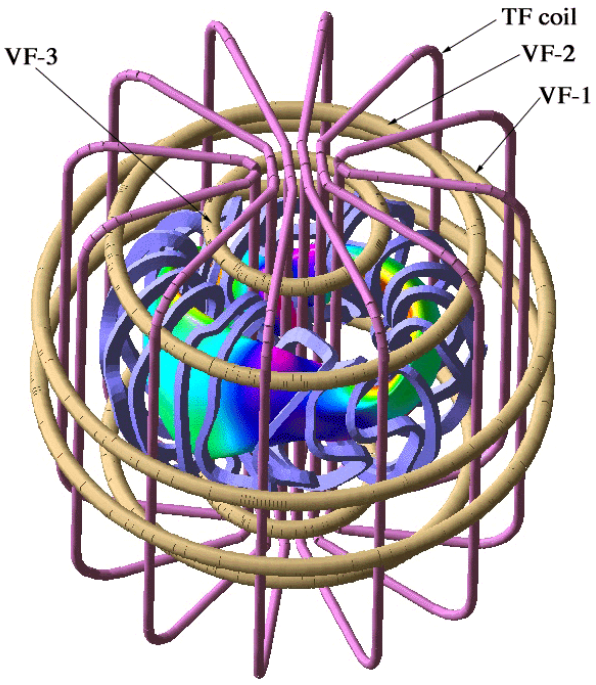

Fig. 1. QPS coil sets and plasma. Modular coils are shown in light blue, toroidal field coils are pink, vertical field coils are in tan. Color contours (blue = low field, red = high field) show the magnetic field strength on the outer plasma magnetic flux surface.

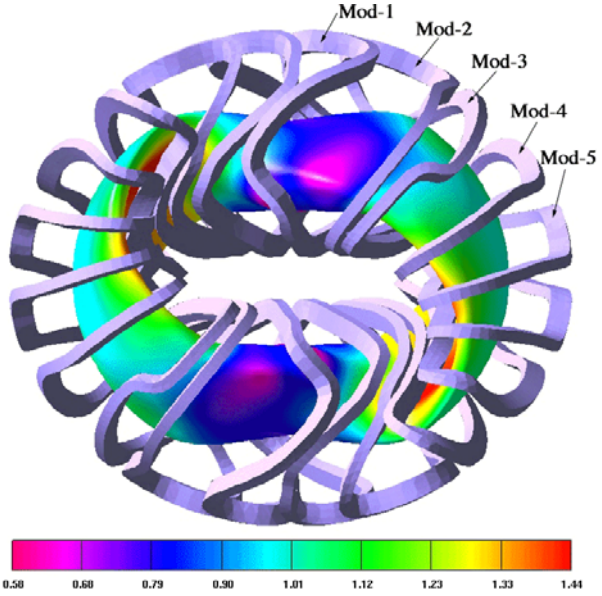

Fig. 2. QPS outer plasma surface and modular magnetic field coils. The colors correspond to the magnitude of the magnetic field.

The coil current optimization will vary the currents in the modular coils, vertical field coils, and toroidal field coils.

Stellarator symmetry is maintained by keeping the currents in each unique modular coil group equal. Engineering constraints will limit the range over which these currents can be varied; the current constraints that we assume are listed in Table 1. These current limits apply to the individual coils in each coil set. Note that in an experimental device, some component of the vertical field coil currents is required for plasma positioning and compensation of stray fields from the Ohmic transformer. We do not directly assess this requirement.

Table 1. Minimum, maximum, and reference current levels for our flexibility study.

Coil	Minimum current (kA)	Maximum current (kA)	Reference design current (kA)
Mod 2	0.0	380.0	300.0
Mod 3	0.0	380.0	300.0
Mod 4	0.0	380.0	300.0
Mod 5	0.0	380.0	300.0
VF1	-60.0	+60.0	0.0
VF2	-180.0	+180.0	-75.5
VF3	-130.0	+130.0	-129.0
TF	-75.0	+75.0	-24.9

Transport optimization

As a first example of coil current optimization, we will find current distributions that can either improve or degrade the neoclassical transport properties of QPS. A number of transport measures are available for this purpose, including the effective ripple from the NEO code [3], collisional transport coefficients from the DKES code [4], quasi-poloidal symmetry, and centering of J^* (longitudinal adiabatic invariant), B_{min}, and B_{max} contours [5]. The primary target that we focus on in this article is the effective ripple calculated by the NEO code. Work is under way on some of the other targets, but is not yet complete. Control over the effective ripple has so far had the most direct correlation with other measures of transport such as DKES and global Monte Carlo lifetime estimates. We have also been able to improve quasi-poloidal symmetry by a factor of 4–5 over the reference design, but this has proven to be anti-correlated with other transport measures. This characteristic may be related to the path that the optimizer chooses for quasi-poloidal symmetry improvement, which is to increase currents in the corner section modular coils (Mod 4,5) and weaken currents in the side modular coils (Mod 2,3). This increases the ripple level and the fraction of trapped particles; over this range of parameters these effects seem to have a more negative impact than the positive effect from the symmetry improvement.

In Fig. 3 the range of effective ripple coefficients obtained by targeting either improved or degraded transport is plotted as a function of flux surface.

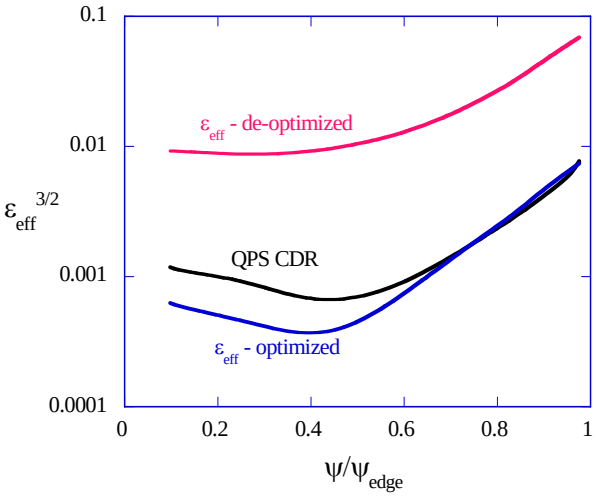

Fig. 3. Effective ripple coefficient as a function of normalized toroidal flux for the reference configuration (QPS CDR) and for improved (red) and degraded (blue) configurations.

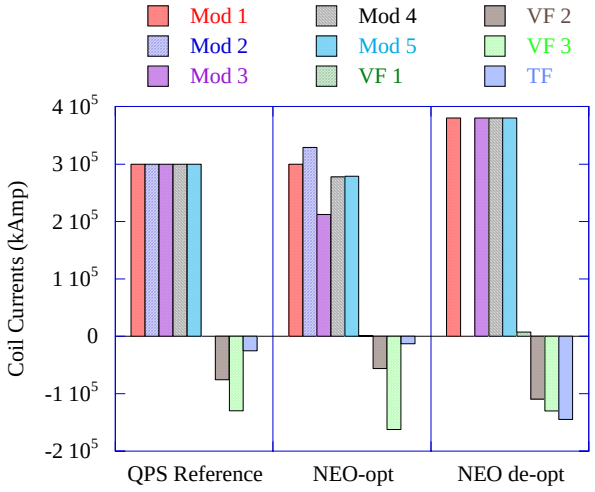

Fig. 4. Coil current distributions for transport optimized and de-optimized cases.

Figure 4 shows a histogram of the coil current distributions that produce the configurations used in Fig. 3. As can be seen, lowered effective ripple is obtained by raising the current in the middle Mod 2 coil and lowering it in the Mod 3, 4, 5 coils going into the corner section. To increase the effective ripple, the optimizer chooses to zero out the current in the Mod 2 coil and run currents in the Mod 1, 3, 4, and 5 coils to their maximum limits (in this case, we allowed currents in all of the modular coils to be varied). Coil–plasma separations have not been significantly changed by these optimizations. For the reference configu-

ration, the minimum coil–plasma separation is 13.2 cm; it becomes 11.9 cm for the NEO optimized case and 13.9 cm for the NEO de-optimized case. These optimizations have been carried out using the Levenberg-Marquardt (LM) option of the STELLOPT optimizer. Coil current optimization attempts have also been made using differential evolution (DE) and genetic algorithm (GA) options. The DE and GA approaches allow the coil current limits to be naturally incorporated into the calculation as bounds on the search process, but to date have not resulted in configurations with good flux surfaces. The LM algorithm does not currently provide any direct way to constrain the values accessed by coil currents; it requires either user intervention or constraint-related targets to accomplish this. Typically we run the LM method for a certain number of iterations, find that one or more of the coil currents has gone outside its acceptable range, fix these coil currents at whichever bound is closest (i.e., maximum/minimum value), restarts the LM algorithm using the reduced number of coils, check again, etc.

The effectiveness of this optimization/de-optimization of transport has been further checked by using other measures of transport. We have run DKES code, [4] which calculates collisional transport coefficients, and the DELTA5DMonte Carlo code [6], which calculates global energy lifetimes.

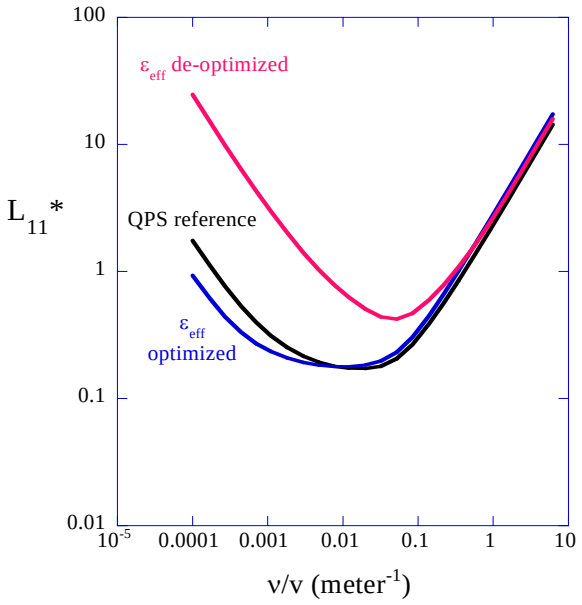

Fig. 5. DKES monoenergetic transport coefficient vs collisionality for the reference, effective ripple optimized, and de-optimized cases (for $E_r = 0$).

In Fig. 5 DKES transport coefficients are plotted for a half radius flux surface and with no radial electric field E_r in order to better show configurational differences. At low collisionalities (below plateau, $\nu/v < 0.02$) these show variations with optimization similar to the effective ripple coefficient shown in Fig. 3. In the higher collisionality regime, there is not as much sensitivity to the configuration.

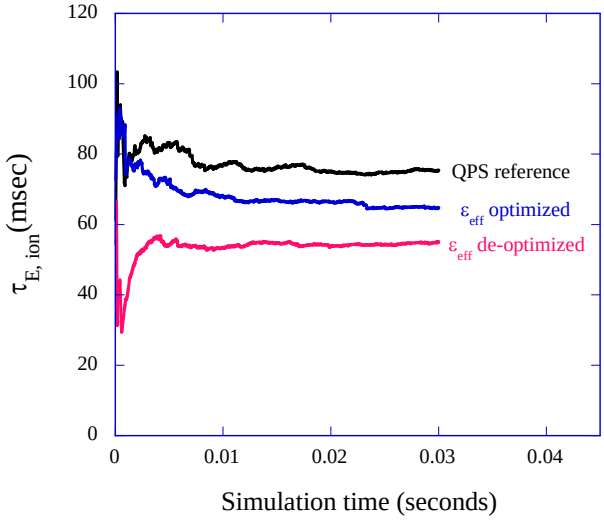

Fig. 6. Monte Carlo global energy lifetimes for reference, transport de-optimized, and optimized configurations.

Figure 6 shows the Monte Carlo ion energy lifetimes for the reference, de-optimized, and optimized configurations for the plasma parameters:
$T_e(0) = 0.5$ keV, $T_i(0) = 0.5$ keV

$$n(0) = 8.3 \times 10^{19}\ \mathrm{m}^{-3}.$$

These parameters are expected to be typical of the QPS ion cyclotron resonance heating (ICRH) regime. This figure indicates that the optimized configuration has lifetimes in between the reference and de-optimized configurations. There is also some tendency towards this behavior in the plateau and higher collisionalities of Fig. 5, but this differs from the low-collisionality behavior. These different trends between the DKES results of Fig. 5 and the Monte Carlo lifetimes are probably related to the different physics content of the two calculations. The Monte Carlo lifetimes do not assume diffusive transport, take into account transport properties over the entire volume, and are based on a Maxwellian distribution; the DKES results of Fig. 5 are monoenergetic and evaluated at a fixed flux surface. Nevertheless, both results show that a significant variation in confinement can be accessed by coil current optimization.

Island avoidance

In addition to variations in the coil currents for confinement optimization, we have carried out similar optimizations in order to control the shape of the rotational transform profile. The goal here has been to use combinations of Ohmically driven plasma current and modifica-

tions in the coil current distributions in order to keep the iota profile bounded between windows determined by the adjacent rational surfaces (which occur for QPS at iota = 2/8, 2/7, 2/6, 2/5, etc.). Once such configurations are found, they are checked by use of the PIES code [7]. If good surfaces are found, then the search ends; if large islands are present, further optimizations are performed to avoid whatever resonance has entered into the plasma. Because there is generally some deviation between the rotational transform predicted by VMEC and that given by PIES, several iterations of this process may be required to find a satisfactory configuration. In the operation of low-aspect-ratio stellarator devices, this type of search for optimum plasma and coil current distributions for island avoidance is expected to be important in finding attractive regimes of operation. It may also be possible to target island reduction more directly through targeting measures such as radial magnetic field components, parallel currents, etc., at the island locations.

We have optimized vacuum configurations with most of the weight placed on the target of attaining a specific rotational transform profile. For the results presented here, the transport properties have then been checked a posteriori, indicating that, in addition to decreased island sizes, the new configurations generally lead to improved confinement. The coil current optimizations have been carried out with varying levels of Ohmic current present; the Ohmic current profile has been modeled as centrally peaked. By combining the coil current optimization with finite plasma current levels, we have been able to both raise the rotational transform profile and flatten it at the same time.

Figure 7 shows some of the VMEC rotational transform profiles that we have obtained by this procedure. Of these profiles, only the 25-kA profile has resulted in good surfaces. The 37-kA profile generated 4/11 islands that destroyed the outer part of the plasma, while the 12-kA case generated 2/7 islands. With further iterations between the optimizer and PIES, it should also be possible to avoid major islands in the 12- and 37-kA cases. Figure 8 shows the coil current distributions that were used to produce the above cases; note that the 12- and 25-kA cases use the same coil currents — only the plasma current has been changed. In Fig. 9, the surfaces obtained from the PIES code are shown for the 25-kA case, indicating that islands have been effectively minimized by this procedure. The 25-kA optimized case had a minimum coil-plasma separation of 14.6 cm as compared to 13.2 cm in the reference case.

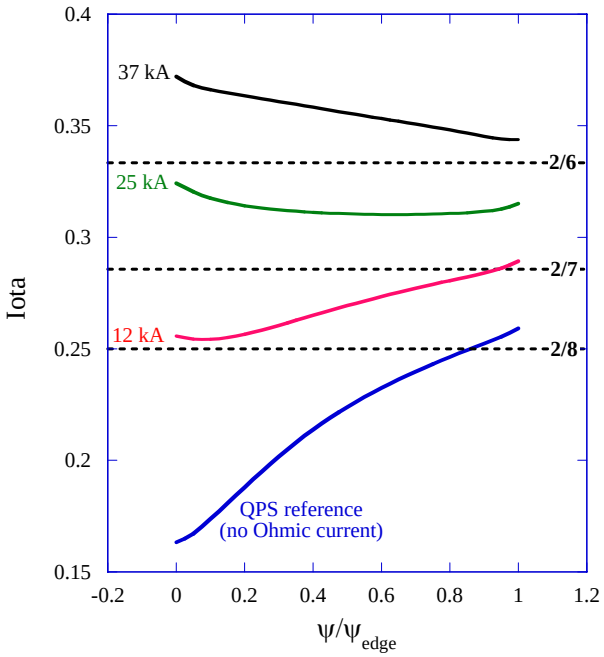

Fig. 7. QPS rotational transform profiles attained through combinations of Ohmic plasma current and coil current optimization.

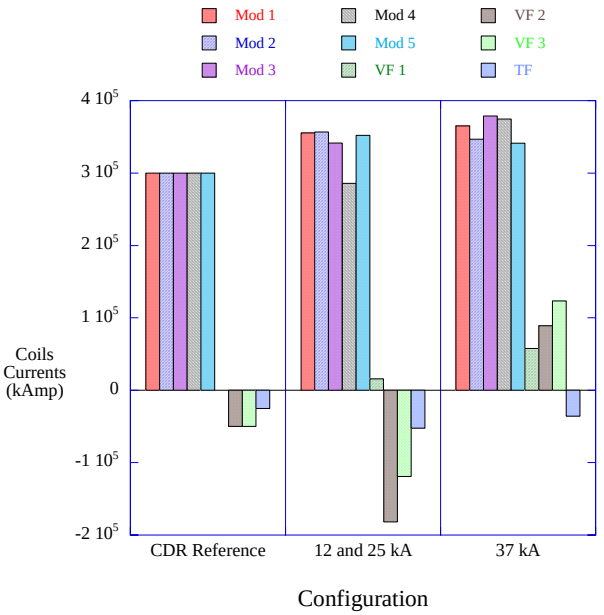

Fig. 8. Coil current distributions for the rotational transform profiles in Fig. 7.

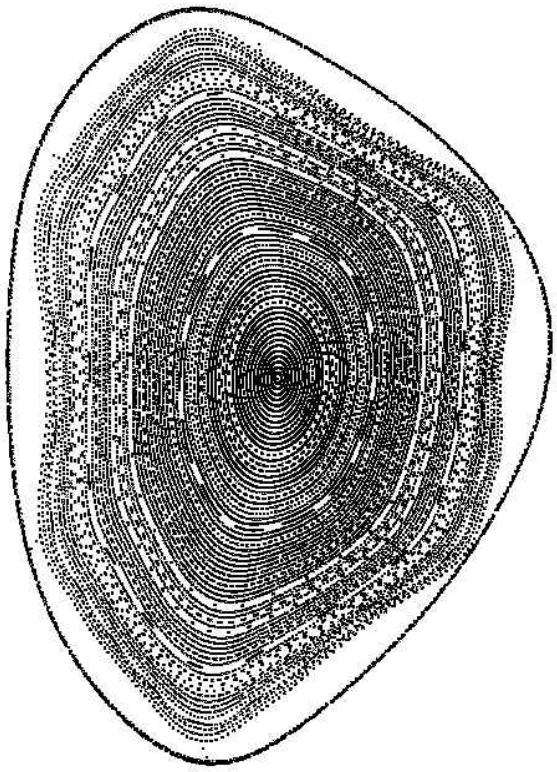

Fig. 9. PIES magnetic surfaces for the coil current optimized case with 25 kA. The transform profile is constrained to remain between the 2/6 and 2/7 resonances.

Conclusions

Physics flexibility is an important aspect of stellarator experiments. We have demonstrated a new way to methodically search for configurations that sample extremes of transport and that minimize low-beta islands using the STELLOPT optimizer. This approach is especially useful when individual modular coil group currents can be varied as well as vertical and toroidal field coil currents. In the case of the QPS device, coil current distributions have been found that result in up to a factor of ~30 variation in low-collisionality transport. Also, the transform profile can be regulated to remain between adjacent rationals, resulting only in island chains of very limited width. Similar techniques should be applicable to other optimization targets, such as stability.

D. A. Spong, D. J. Strickler, S. P. Hirshman, J. F. Lyon, L. A. Berry, D. Mikkelsen,[1] D. Monticello,[1] A. S. Ware[2]
Oak Ridge National Laboratory, P.O. Box 2009, Oak Ridge, TN 37831-8073

[1]Princeton Plasma Physics Laboratory, P.O. Box 451, Princeton, NJ 08502

[2]Department of Physics and Astronomy, University of Montana, Missoula, MT, 59812

References

[1] D. J. Strickler et al., to be published in Fusion Science and Technology, 2003.

[2] J. F. Lyon et al., "Overview of the QPS Project," and D. A. Spong et al., "Confinement Physics of Quasi-Poloidal Stellarators," 30th European Physical Society Conf. on Controlled Fusion and Plasma Physics, St. Petersburg, Russia, July 7–11, 2003.

[3] V. V. Nemov, S. V. Kasilov, W. Kernbichler, and M. F. Heyn, Phys. Plasmas **6**, 4622 (1999).

[4] W. I. van Rij, S. P. Hirshman, Phys. Fluids B **1** (1989).

[5] J. A. Rome, Nucl. Fusion **35**, 195 (1995).

[6] D, A. Spong, S. P. Hirshman, L. A. Berry, J. F. Lyon, et al., Nucl. Fusion **41**, 711 (2001).

[7] A. Reiman and H. S. Greenside, J. Comput. Phys. **75**, 423 (1988).

Recent results for ECH plasmas in Heliotron J

Heliotron J device

Heliotron J is a medium-sized plasma experimental device at the Institute of Advanced Energy, Kyoto University, Japan. It was designed and constructed in FY2000 as a first step towards an optimized helical-axis heliotron. One of the objectives of the device is to explore the properties of the nonsymmetric, quasi-omnigeneous optimization for heliotrons, thus leading to the establishment of better design principles. The experimental program is organized to study high-level compatibility between good particle confinement and MHD stability, as well as its divertor scheme under small bootstrap current conditions. The device parameters are as follows: the major plasma radius is 1.2 m, the average plasma minor radius is 0.1–0.2 m, and the magnetic field strength on the magnetic axis is < 1.5 T. The vacuum rotational transform is 0.3–0.8 with low magnetic shear, and a magnetic well depth of 1.5% at the plasma edge. Heliotron J has several heating systems, namely 0.5-MW electron cyclotron heating (ECH), 1.5-MW neutral beam injection (NBI), and 2.0-MW ion cyclotron heating (ICH).

Energy confinement characteristics

A schematic view of Heliotron J is shown in Fig. 1. The 70-GHz electron cyclotron heating (ECH) system has a well-focused Gaussian beam and a flexible launching system to control the beam direction both toroidally and poloidally. The maximum injection power is about 0.4 MW, and a ray tracing calculation has been used to estimate the single-pass absorption efficiency [1]. For the perpendicular injection case, optimal heating with regard to the attainable plasma stored energy was realized when the second harmonic resonance layer was located near the magnetic axis (B_0 = 1.25 T). The stored energy at an ECH injection power of 0.3 MW increased with density to 2.5 kJ at a line-averaged density of 2.5×10^{19} m^{-3}. As the line-averaged density further approached the ECH cut-off density of 3.0×10^{19} m^{-3}, the plasma energy content began to decrease. The global energy confinement times when the energy content is at its peak have been compared with that of the ISS95 scaling. As shown in Fig. 2, it was found that there existed good confinement plasmas whose confinement times were 1.5–2 times better than the ISS95 scaling.

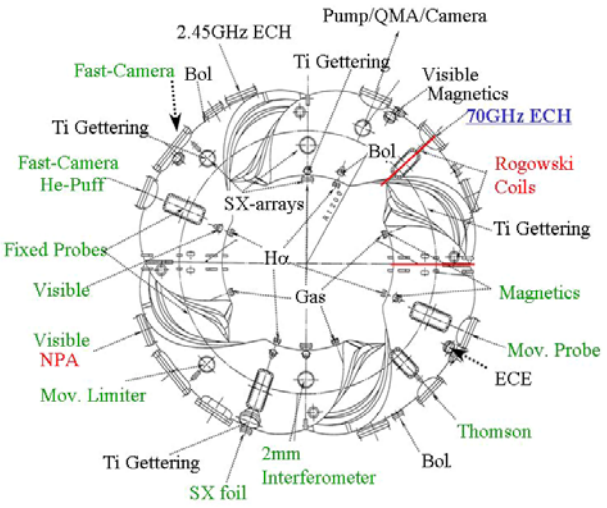

Fig. 1. Top view of Heliotron-J showing the major diagnostic locations.

A spontaneous transition of the confinement state, like that of H-mode, was observed during ECH with strong gas puffing at electron densities above a certain threshold value, as shown in Fig. 3 [2]. At this transition, sudden drops in H_α and scrape-off layer (SOL) density signals and subsequent strong rises in line-averaged density and in plasma energy content were observed. Electron cyclotron emission (ECE) measurements revealed that, after the transition, the core electron temperature inside $r/a < 2/3$ is well maintained or a little increased despite the strong increase in density. In the SOL region, Langmuir probe measurements revealed that the SOL density fluctuation also drops in the frequency range below 200 kHz after the transition.

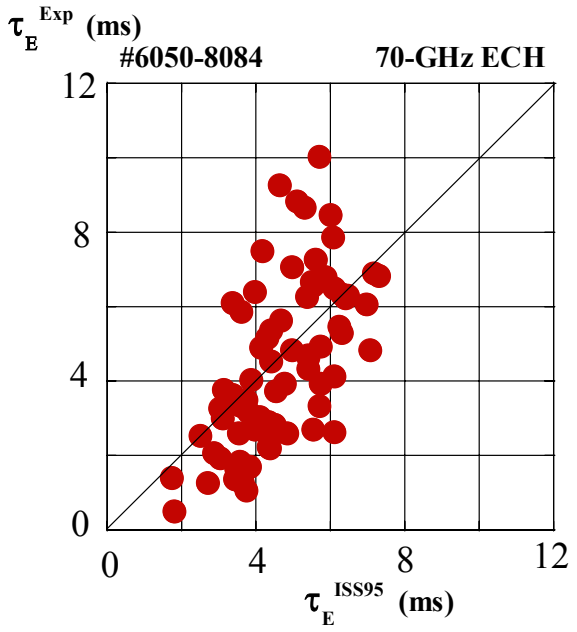

Fig. 2. Experimental peak global energy confinement time as a function of the ISS95 scaling law.

From iota-scan experiments carried out by controlling the auxiliary vertical coil current, two edge iota windows for this spontaneous confinement transition were discovered. One window [$0.54 < i(a)/2\pi < 0.56$] was obtained in a separatrix discharge, and the other window [$0.62 < i(a)/2\pi < 0.63$] was obtained in a partial wall-limiter discharge. A VMEC equilibrium calculation predicts that the change of the edge iota value at averaged beta values less than 0.3% is < (–)0.020. The change of the edge iota value at measured bootstrap currents of < 2 kA is < (+)0.015. These changes are compensatory so that we choose the vacuum edge iota value as a reference. The boundaries of these two edge iota windows are near the natural resonances of the Heliotron J configuration, such as (i) the intrinsic $n = 4$, $m = 7$ (fourfold symmetry of Heliotron J), (ii) $n = 8$, $m = 13$ and 15, and (iii) $n = 12$, $m = 19$, where m and n are the poloidal and toroidal mode number, respectively.

For edge iota $i(a)/2\pi = 0.542$, the peak increment of the plasma energy content reached about 70%. However, at present, this confinement improvement remains transient on an energy confinement time scale and the post-transition steady-state phase has not been reached yet. As for the threshold density, the minimum threshold line-averaged density for 0.3-MW ECH was found to be rather low, $\bar{n}_e = 1.2\text{–}1.6 \times 10^{19}$ m^{-3}.

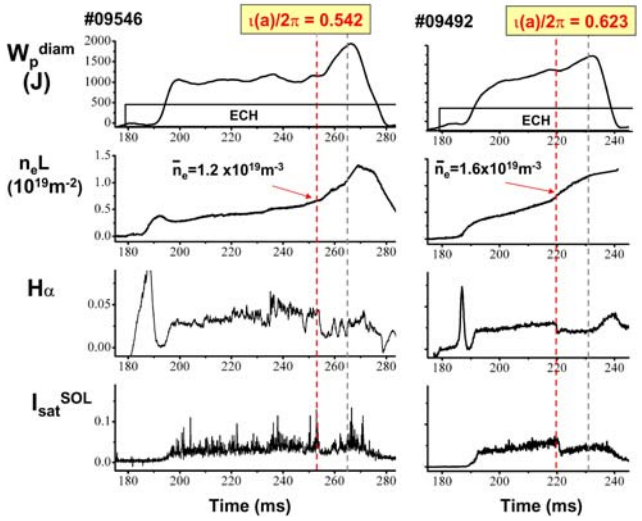

Fig. 3. Spontaneous transition of confinement improvement during ECH for the two edge iota windows: $\iota(a)/2\pi = 0.542$ and $\iota(a)/2\pi = 0.623$.

Toroidal current control

In helical systems, the bootstrap current can be controlled to be approximately zero or very small by changing the Fourier components of the magnetic field spectrum. In addition to the helicity and toroidicity, as a third parameter, "bumpiness," is also expected to control the bootstrap current in Heliotron J. In this study, the toroidal current behavior for perpendicular ECH discharges was studied by changing the bumpiness using the inner vertical coil.

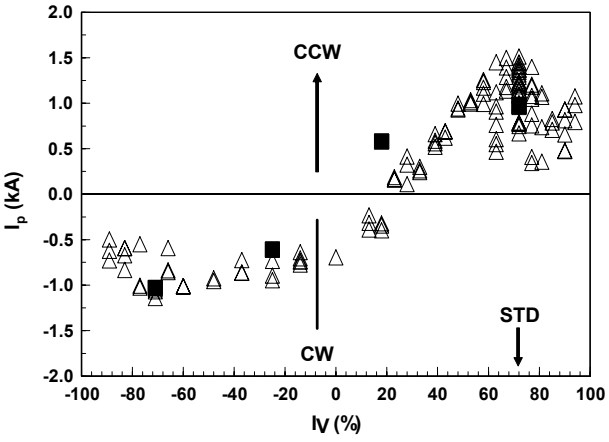

Fig. 4. The toroidal current dependence on the configuration as controlled by the inner vertical coil current. Squares are the results of the theoretical calculation.

Figure 4 shows the dependence of the toroidal current on the coil current of the inner vertical coil [3]. This control method mainly varies the bumpy component of the magnetic field spectrum. In this figure, current that flows in the counterclockwise direction (as viewed from the top of Heliotron J) is expressed as positive current. With this def-

inition, positive toroidal current increases the poloidal magnetic field. In this experiment, the magnetic field strength was adjusted so that the second harmonic resonance (1.25 T) was located at the plasma center. When the inner vertical coil current decreased, the toroidal plasma current decreased and finally reversed. The measured current was in the range of 1–1.5 kA for $\bar{n}_e = 1.0 \times 10^{19}$ m^{-3}. For the maximum current of 2.5 kA, which was obtained at a higher density ($\bar{n}_e = 1.5 \times 10^{19}$ m^{-3}) in the standard configuration (STD), the equilibrium calculation predicts that $\iota(a)/2\pi$ is increased by 0.02. When the confinement field was reversed, the plasma current I_p also reversed direction, but its magnitude remained almost the same. These characteristics agreed with those expected for the neoclassical bootstrap current. The amount of the plasma current is also within the range expected from the theoretical calculation [4], indicated by squares in Fig. 4.

An experiment with electron cyclotron current drive (ECCD) was carried out to clarify the control of the toroidal current [3]. By changing the toroidal injection angle of electron cyclotron (EC) waves using a steering mirror system, the toroidal current could be varied from 1 kA to 0.6 kA if the density was less than 0.5×10^{19} m^{-3} and the effect of the bootstrap current was small. In the higher density case around 1.0×10^{19} m^{-3}, EC current was also observed. These experimental results demonstrate the capability of toroidal current control by ECCD in Heliotron J.

Observation of high-energy ions in ECH plasmas

In order to investigate the properties of the high-energy ions in Heliotron J, a charge-exchange neutral particle analyzer (CX-NPA) has been installed. Details of the CX-NPA system are reported in Ref. [5].

Figure 5 shows a typical energy spectrum obtained in ECH plasmas for low ($\bar{n}_e \approx 0.2 \times 10^{19}$ m^{-3}) and middle ($\bar{n}_e \approx 1.1 \times 10^{19}$ m^{-3}) density. In the middle-density case, the energy spectrum seems to be a single Maxwellian distribution, while a folded spectrum has been observed in the low-density case. The measured energy spectrum in the middle-density case is consistent with that calculated when the ion energy distribution function is assumed to be a Maxwellian distribution with a temperature of 190 eV at the center, and a parabolic profile. In the low-density case, on the other hand, the calculated spectrum with a single Maxwellian cannot explain the measured spectrum. When a high-energy component with the effective temperature of 1500 eV is included, assuming that the ratio of the density of this component to the total ion density is 18%, the expected spectrum agrees well with the experiment (a bold solid line in Fig. 5). It was found that the "effective" temperature of the high-energy component increased with decreasing density and with injection power of ECH.

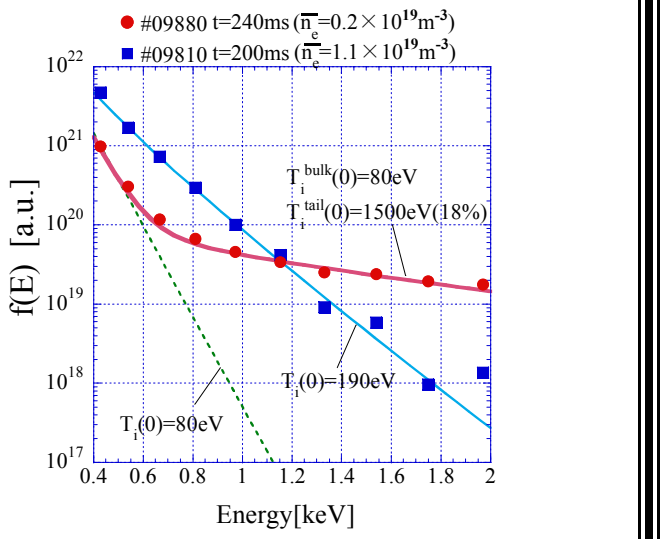

Fig. 5. Typical charge exchange energy spectra in ECH plasmas showing a high-energy tail at low densities.

Such a high energy component in the ECH/ECCD plasmas has been observed in several toroidal devices [6, 7]. The phenomenon has been discussed in relation to the additional anomalous wave heating or coupling of the high-energy electrons to the ions. However, the mechanism of the production of the high-energy ions has not been identified yet.

S. Kobayashi,[1] H.Okada,[1] K. Nagasaki,[1] T. Mizuuchi,[1] S. Yamamoto,[1] K. Hanatani,[1] Y. Nakamura,[2] M. Nakasuga,[2] K. Kondo,[2] F. Sano,[1] V. Tribaldos,[3] and T. Obiki[1]

1. Institute of Advanced Energy, Kyoto University, Gokasho, Uji, Japan.
2. Graduate School of Energy Science, Kyoto University, Yoshida-honmachi, Kyoto, Japan.
3. Laboratorio Nacional de Fusión, Asociación EURATOM-CIEMAT, Madrid, Spain.

References

[1] V. Tribaldos et al., J. Plasma Fusion Res. **78** (2002) 996–997.

[2] F. Sano et al., "Characterization of ECH plasma confinement in Heliotron J," paper O-2.2A presented at the 30th EPS Conf. On Controlled Fusion and Plasma Physics, St. Petersburg, 2003 (proceedings to be published in Europhys. Conf. Abstr. **27A)**.

[3] H. Okada et al., "Studies on toroidal current in Heliotron J," paper P-3.27 presented at the 30th EPS Conf. On Controlled Fusion and Plasma Physics, St. Petersburg, 2003 (proceedings to be published in Europhys. Conf. Abstr. **27A)**.

[4] K.Y. Watanabe et al., Nucl. Fusion **41** (2001) 74.

[5] M. Kaneko et al., “Charge-exchange neutral particle measurements in helical-axis Heliotron J,” paper P-3.28 presented at the 30th EPS Conf. On Controlled Fusion and Plasma Physics, St. Petersburg, 2003 (proceedings to be published in Europhys. Conf. Abstr. **27A)**.

[6] V. Erckmann et al., Plasma Phys. Control. Fusion **36** (1994) 1896.

[7] Z. A.Pietrzyk et al., Nucl. Fusion **33** (1993) 197.